Modelling inelastic granular media using Dynamical Density Functional Theory

Noname manuscript No.
(will be inserted by the editor)

Modelling inelastic granular media using Dynamical Density Functional Theory

B. D. Goddard · T. D. Hurst · R. Ocone

Received: date / Accepted: date

Abstract We construct a new mesoscopic model for granular media using Dynamical Density Functional Theory (DDFT). The model includes both a collision operator to incorporate inelasticity and the Helmholtz free energy functional to account for external potentials, interparticle interactions and volume exclusion. We use statistical data from event-driven microscopic simulations to determine the parameters not given analytically by the closure relations used to derive the DDFT. We numerically demonstrate the crucial effects of each term and approximations in the DDFT, and the importance of including an accurately parametrised pair correlation function.

Keywords Granular media · Dynamical Density Functional Theory

1 Introduction

Granular media is ubiquitous in industrial and natural processes [4,50], but very difficult to accurately model in large systems. Microscopic models [13,7] generally produce accurate results, but are usually restricted to simple systems, a relatively small number of particles, or short simulation times. This is due to computational cost scaling poorly with the number of particles in the

B.D.Goddard
School of Mathematics and the Maxwell Institute for Mathematical Sciences, University of Edinburgh, Edinburgh, UK, EH9 3FD
E-mail: b.goddard@ed.ac.uk

T. D. Hurst
School of Mathematics and the Maxwell Institute for Mathematical Sciences, University of Edinburgh, Edinburgh, UK, EH9 3FD
E-mail: t.hurst@sms.ed.ac.uk

R. Ocone
School of Engineering and Physical Sciences, Heriot-Watt University, Edinburgh, UK, EH14 4AS
E-mail: r.ocone@hw.ac.uk

system. In industrial processes such as fluidisation [19] there can be as many $\mathcal{O}(10^{30})$ particles interacting at a microscopic level, which can change the fluid behaviour of the system. Through coarse-graining methods [46,54,48] and by implementing state-of-the-art numerical algorithms on modern supercomputers, microscopic simulations can model billions of particles, but it is generally difficult to simulate such a number of over long time frames, and this is many magnitudes below the number of particles in full physical systems.

Models which approximate the media as a macroscopic continuum [34,56] are not inhibited by the number of particles in the system. However, continuum models need to be supplied with constitutive equations for bulk properties, such as the particle stress tensor. Such constitutive equations, in the dilute flow regime are usually obtained by invoking the kinetic-collisional theory [34]. The disadvantages of such constitutive equations lie mainly in what is believed to be its inability to treat the meso-scale: issues such as cluster formation (and breakage), for instance, have been discussed at large [31], and attempts to solve those issues have been proposed (e.g., by "adjusting" the Navier-Stokes equations [31,41]).

Recently, approaches using Dynamical Density Functional Theory (DDFT) have produced promising results in the field of modelling complex fluids [38,3, 37] at a *mesoscopic* level. Derived from a particle-based model, DDFTs are continuum models that utilise the well-studied Helmholtz free energy functional [25] and can include interparticle and external potentials, volume exclusion [53], hydrodynamic interactions [49,23] and multiple species [21]. However, current models do not account for inelastic (or indeed elastic) collisional dynamics, which have crucial dissipative effects in granular media.

We introduce a DDFT adapted for granular media in Section 2 which incorporates particle collisions at the mesoscopic level. In section 2.4, we discuss how we approximate parameters of the system to close the continuum model, in particular the radial correlation function. Following this we present some numerical results in Section 3: we construct the radial correlation function under the assumptions of the model, and perform particle and DDFT simulations for a one dimensional example, to show the effects of each term in the DDFT and any approximations that have been considered. There are many areas for further investigation, which we discuss at the end of this paper.

2 Derivation of the model

2.1 Microscopic Dynamics

A set of N particles, each of mass m, in d dimensions can be modelled via Langevin [16] or Newton equations of motion. We set $\boldsymbol{r}_i \in \mathbb{R}^d, \boldsymbol{p}_i \in \mathbb{R}^d$ as the position and velocity of particle i for $i = 1, \ldots, N$. We then define $\boldsymbol{r}^N = (\boldsymbol{r}_1, \boldsymbol{r}_2, ..., \boldsymbol{r}_N)$ $\boldsymbol{p}^N = (\boldsymbol{p}_1, \boldsymbol{p}_2, ..., \boldsymbol{p}_N)$ as the concatenation of all particle positions and momenta respectively. The dynamics of $\boldsymbol{r}^N$ and $\boldsymbol{p}^N$ are then

given by

$$\frac{\mathrm{d}\boldsymbol{r}^N}{\mathrm{d}t} = \frac{\boldsymbol{p}^N}{m}, \quad \frac{\mathrm{d}\boldsymbol{p}^N}{\mathrm{d}t} = -\boldsymbol{\nabla}_{\boldsymbol{r}^N} V(\boldsymbol{r}^N, t) - \gamma \boldsymbol{p}^N + \boldsymbol{a}(t), \tag{1}$$

where

$$V(\boldsymbol{r}^N, t) = \sum_{i=1}^{N} V_{\mathrm{ext}}(\boldsymbol{r}_i, t) + \frac{1}{2}\sum_{i\neq j=1}^{N} V_2(\boldsymbol{r}_i, \boldsymbol{r}_j) + \frac{1}{6}\sum_{i\neq j\neq k=1}^{N} V_3(\boldsymbol{r}_i, \boldsymbol{r}_j, \boldsymbol{r}_k) + \cdots . \tag{2}$$

Here $V_{\mathrm{ext}}(\boldsymbol{r}_i, t)$ represents any external potential, for example gravity. Pairwise interactions are modelled by an interparticle potential $V_2(\boldsymbol{r}_i, \boldsymbol{r}_j)$ for $i, j = 1, ..., N$, and we analogously include higher order interparticle potentials such as $V_3(\boldsymbol{r}_i, \boldsymbol{r}_j, \boldsymbol{r}_k)$ for $i, j, k = 1, ..., N$. The second term on the right hand side of the equation for momentum in eq. (1) represents external frictional effects, for example if the particles are moving in a bath, where $\gamma > 0$ determines the strength of the effect. The final term $\boldsymbol{a}(t)$ is a Brownian motion term [10] from thermal fluctuations in the bath, with strength $(mk_BT\gamma)^{1/2}$ determined by a fluctuation-dissipation theorem [17], where k_B is Boltzmann's constant and T is the bath temperature. Granular media particles are usually assumed to be unaffected by thermal fluctuations, however for modelling purposes this term is sometimes included as a thermostat [39].

For point-like particles, eq. (1) fully describes the dynamics of the system. In contrast, in this paper we assume that particles are spherical with diameter σ. We include the effects of collisions in the dynamics of particles by restricting their movement to the *hard sphere domain*:

$$\mathcal{D}_N = \{\boldsymbol{r}^N, \boldsymbol{p}^N \in \mathbb{R}^{dN} : \forall i, j, \|\boldsymbol{r}_i - \boldsymbol{r}_j\| \geq \sigma\}. \tag{3}$$

When two particles that are moving toward one another come into contact, we must then instantaneously change their momenta to avoid particle overlap. We assume that collisions are binary and instantaneous; *i.e.* a collision between the i^{th} and j^{th} particles occurs at time t if $\|\boldsymbol{r}_i(t) - \boldsymbol{r}_j(t)\| = \sigma$, and $(\boldsymbol{p}_i(t) - \boldsymbol{p}_j(t)) \cdot (\boldsymbol{r}_i(t) - \boldsymbol{r}_j(t)) < 0$. To resolve the collision we apply a *collision rule*. A standard collision rule which maps pre-collisional velocities $\boldsymbol{p}_i^{\mathrm{in}}, \boldsymbol{p}_j^{\mathrm{in}}$ to post-collisional velocities $\boldsymbol{p}_i^{\mathrm{out}}, \boldsymbol{p}_j^{\mathrm{out}}$ is given by [6]:

$$\boldsymbol{p}_i^{\mathrm{out}} = \boldsymbol{p}_i^{\mathrm{in}} - \frac{(1+\alpha)}{2}\boldsymbol{\nu}^{i,j} \cdot (\boldsymbol{p}_i^{\mathrm{in}} - \boldsymbol{p}_j^{\mathrm{in}})\boldsymbol{\nu}^{i,j}, \quad \boldsymbol{p}_j^{\mathrm{out}} = \boldsymbol{p}_j^{\mathrm{in}} + \frac{(1+\alpha)}{2}\boldsymbol{\nu}^{i,j} \cdot (\boldsymbol{p}_i^{\mathrm{in}} - \boldsymbol{p}_j^{\mathrm{in}})\boldsymbol{\nu}^{i,j}, \tag{4}$$

where $\boldsymbol{\nu}^{i,j} = (\boldsymbol{r}_i - \boldsymbol{r}_j)/\|\boldsymbol{r}_i - \boldsymbol{r}_j\|$ and $\alpha \in (0, 1]$ is the coefficient of restitution. If $\alpha = 1$, the collisions are perfectly elastic and no energy is dissipated, and the component of velocity in the direction of the collision is reflected. If $\alpha < 1$, energy is lost via a reduction of the velocity component in the direction of the

collision. We note that linear and angular momentum are conserved by this collision rule:

$$\boldsymbol{p}_i^{\text{out}} + \boldsymbol{p}_j^{\text{out}} = \boldsymbol{p}_i^{\text{in}} + \boldsymbol{p}_j^{\text{in}}, \tag{5}$$

$$(\boldsymbol{r}_i - \boldsymbol{x}) \times \boldsymbol{p}_i^{\text{out}} + (\boldsymbol{r}_j - \boldsymbol{x}) \times \boldsymbol{p}_j^{\text{out}} = (\boldsymbol{r}_i - \boldsymbol{x}) \times \boldsymbol{p}_i^{\text{in}} + (\boldsymbol{r}_j - \boldsymbol{x}) \times \boldsymbol{p}_j^{\text{in}}, \quad \forall \boldsymbol{x} \in \mathbb{R}^3. \tag{6}$$

However, kinetic energy is not conserved when $\alpha < 1$:

$$\|\boldsymbol{p}_i^{\text{out}}\|^2 + \|\boldsymbol{p}_j^{\text{out}}\|^2 \leq \|\boldsymbol{p}_i^{\text{in}}\|^2 + \|\boldsymbol{p}_j^{\text{in}}\|^2 \tag{7}$$

For simplicity, in this derivation we do not investigate the effect of angular momentum on the DDFT model [15] when collisional effects are included.

In principle, eq. (1), on the domain presented in eq. (3) with collision rule eq. (4) can accurately model a system of N particles. Particle based methods can produce very accurate results, but for N up to $\mathcal{O}(10^9)$, or when the system is very dense, reaching the desired simulation time is generally infeasible, or the simulation becomes too memory-intensive. Furthermore, when $\alpha < 1$ a system of particles obeying the above microscopic dynamics can experience inelastic collapse, where an infinite number of collisions can occur in finite time, effectively jamming simulations [40].

2.2 N-body equations for rigid particles

If collisions are neglected, associated with eq. (1) is the *Kramer's equation* (or in absence of thermal fluctuations, the *Liouville equation*) [51], a partial differential equation (PDE) which models the dynamics of the N-particle distribution function $f^{(N)}(\boldsymbol{r}^N, \boldsymbol{p}^N, t)$, the probability of finding N particles with positions $\boldsymbol{r}^N$ and momenta $\boldsymbol{p}^N$ at time t:

$$\left[\frac{\partial}{\partial t} + \frac{1}{m}\boldsymbol{p} \cdot \boldsymbol{\nabla}_{\boldsymbol{r}^N} - \boldsymbol{\nabla}_{\boldsymbol{r}^N} V(\boldsymbol{r}^N, t) \cdot \boldsymbol{\nabla}_{\boldsymbol{p}^N}\right] f^{(N)}(\boldsymbol{r}^N, \boldsymbol{p}^N, t) - \boldsymbol{\nabla}_{\boldsymbol{p}^N} \cdot \left[\gamma(\boldsymbol{p}^N + mk_BT\boldsymbol{\nabla}_{\boldsymbol{p}^N}) f^{(N)}(\boldsymbol{r}^N, \boldsymbol{p}^N, t)\right] = 0. \tag{8}$$

When constructing eq. (8) for deterministic dynamics, the microscopic dynamics are assumed to be smooth. However, particles which undergo instantaneous collisions have discontinuities in their velocity profile, and so their trajectories are not smooth. In [57], the *weak formulation* of the Liouville equation is constructed for a system of elastic spherical particles that obey linear dynamics, using distribution theory.

In [57], the author argues that the Liouville equation cannot be applied to collisional dynamics in a rigorous sense, as individual particle trajectories are not smooth. As an alternative, they derive the Liouville equation in its weak form, by first applying the Liouville equation to a test function, then multiplying by the particle distribution $f^{(N)}$ (which obeys the necessary identities

to ensure that collisions are correctly resolved) and integrating with respect to all spatial, velocity, and temporal dimensions. This enables the application of various integration identities, which moves the Liouville operator over to the particle distribution function, while also accounting for collisional dynamics.

Without any additional assumptions, careful dissection of the phase space via $f^{(N)}$ leads to an additional collisional term (in the weak sense) on the right-hand side of eq. (8):

$$C[f^{(N)}] = \int_{\partial\mathcal{D}_N(\boldsymbol{r}_1,t)} \int_{\mathbb{R}^{dN}} f^{(N)}(\boldsymbol{r}^N, \boldsymbol{p}^N, t)\boldsymbol{p}^N \cdot \hat{\boldsymbol{n}} \, \mathrm{d}\boldsymbol{p}^N \, \mathrm{d}\mathcal{H}(\boldsymbol{r}), \tag{9}$$

where for $k \leq N$,

$$\mathcal{D}_N(\boldsymbol{r}^k, t) = \{\boldsymbol{r}^{N-k} \in \mathbb{R}^{d(N-k)}, \boldsymbol{p}^N \in \mathbb{R}^{dN} : \forall i, j, \|\boldsymbol{r}_i - \boldsymbol{r}_j\| \geq \sigma\}, \tag{10}$$

and $\hat{\boldsymbol{n}}$ is the outward unit normal of $\partial\mathcal{D}_N(\boldsymbol{r}_1, t)$ with $\mathcal{H}(\boldsymbol{r}^N)$ the Hausdorff measure on $\partial\mathcal{D}_N(\boldsymbol{r}_1, t)$. The result has been derived for a system of $N = 2$ particles that have linear trajectories and collide elastically. In [29] the result is then extended to account for general interaction forces and particle trajectories. Under the assumption that collisions are binary and well-separated, the result should also be appropriate for systems of N particles. We do not go into any more explicit detail here, but refer the reader to the derivations in [57, 29]

When considering the associated Bogoliubov-Born-Green-Kirkwood-Yvon (BBGKY) hierarchy [5] (in weak form), the additional term integrates to the well-known Boltzmann collision operator for $\alpha = 1$, and when $\alpha > 1$ we can derive its inelastic counterpart:

$$\begin{aligned}\mathcal{L}_{\text{coll}}(f^{(2)}) =& \sigma^{d-1} \int_{\mathbb{R}^d} \mathrm{d}\boldsymbol{p}_2 \int_{\mathbb{S}^{d-1}} \mathrm{d}\boldsymbol{\omega} \chi_{(\boldsymbol{p}_1-\boldsymbol{p}_2)\cdot\boldsymbol{\omega}>0}(\boldsymbol{p}_1 - \boldsymbol{p}_2) \cdot \boldsymbol{\omega} \times \\ & \left[\frac{1}{\alpha^2} f^{(2)}(\boldsymbol{r}_1, \boldsymbol{r}_1 - \sigma\boldsymbol{\omega}, \boldsymbol{p}_1, \boldsymbol{p}_2, t) - f^{(2)}(\boldsymbol{r}_1, \boldsymbol{r}_1 + \sigma\boldsymbol{\omega}, \boldsymbol{p}_1', \boldsymbol{p}_2', t)\right],\end{aligned} \tag{11}$$

where $\boldsymbol{p}_i'$ is the pre-collisional velocity associated to $\boldsymbol{p}_i$, determined using eq. (4). Thus the BBGKY hierarchy can be derived rigorously in its weak form. We note that this is an alternative method to derivations where the collision term is constructed by additional assumptions on an interaction force at the level of the BBGKY hierarchy [27].

Equation (8) (or an analogous weak formulation including eq. (9)) replaces a system of $2N$ differential equations with a single PDE. However $f^N(\boldsymbol{r}^N, \boldsymbol{p}^N, t)$ is defined on a region in a $2dN + 1$ dimensional space. If we were to simulate this system on a discretized domain with M points in each direction, we would require M^{2dN} points for simulation, which quickly becomes computationally intractable.

To derive a computationally efficient model for use in simulation, we can rely on the result of [11], which relates the N-particle distribution function

and the one-body position density as follows:

$$\rho(\boldsymbol{r}_1, t) = N \int_{\mathbb{R}^{(N-1)d}} \int_{\mathbb{R}^{Nd}} \mathrm{d}\boldsymbol{p}^N \, \mathrm{d}\boldsymbol{r}^{N-1} f^{(N)}(\boldsymbol{r}^N, \boldsymbol{p}^N, t) \chi_{\mathcal{D}_N(\boldsymbol{r}^1, t)}. \tag{12}$$

We include the characteristic function to stress that the phase space of the system does not allow particles to overlap, ensuring that we integrate over the hard-sphere domain while keeping the first position variable free. In contrast, in derivations where particles interact purely via soft potentials, the integral in position is over $\mathbb{R}^{d(N-1)}$. Heuristically, when integrating eq. (8) the inclusion of this characteristic function leads to collisional terms in the BBGKY hierarchy. Rigorously, the Boltzmann collision operator is a consequence of additional terms in the weak formulation of the Liouville equation, after integrating out all but one particle position and velocity, and the inclusion of the characteristic function in the derivation is a natural consequence of the weak form.

To arrive at an equation to model $\rho(\boldsymbol{r}, t)$ we first define the *n-reduced phase space particle distribution function* by

$$f^{(n)}(\boldsymbol{r}^n, \boldsymbol{p}^n, t) = \frac{N!}{(N-n)!} \int_{\mathbb{R}^{(N-n)d}} \int_{\mathbb{R}^{(N-n)d}} \mathrm{d}\boldsymbol{r}^{(N-n)} \, \mathrm{d}\boldsymbol{p}^{(N-n)} f^{(N)}(\boldsymbol{r}^N, \boldsymbol{p}^N, t) \chi_{\mathcal{D}_N(\boldsymbol{r}^n, t)}, \tag{13}$$

where $\boldsymbol{r}^{N-n} = (\boldsymbol{r}_{n+1}, ..., \boldsymbol{r}_N)$, $\boldsymbol{r}^n = (\boldsymbol{r}_1, \boldsymbol{r}_2, ..., \boldsymbol{r}_n)$, and similar for $\boldsymbol{p}^{N-n}, \boldsymbol{p}^n$. To ease notation in the derivation we write $\boldsymbol{r} = \boldsymbol{r}_1$, $\boldsymbol{p} = \boldsymbol{p}_1$. By integrating eq. (8) with respect to $\boldsymbol{r}^{N-1}$ and $\boldsymbol{p}^{N-1}$, and appealing to the symmetry of arguments in $f^{(N)}$, we arrive at the *one-body Kramer's equation*, the first equation in the BBGKY hierarchy:

$$\begin{aligned} \frac{\partial f^{(1)}}{\partial t} + \frac{1}{m} \boldsymbol{p} \cdot \boldsymbol{\nabla}_{\boldsymbol{r}} f^{(1)} - \boldsymbol{\nabla}_{\boldsymbol{r}} V^{ext}(\boldsymbol{r}, t) \cdot \boldsymbol{\nabla}_{\boldsymbol{p}} f^{(1)} - \boldsymbol{\nabla}_{\boldsymbol{p}} \cdot \left[\gamma(\boldsymbol{p} + m k_B T \nabla_{\boldsymbol{p}}) f^{(1)} \right] \\ - \frac{1}{m} \mathcal{L}_{\mathrm{coll}}(f^{(2)}) - \mathcal{L}_{\mathrm{part}}(f^{(2)}, f^{(3)}, ..., f^{(N)}) = 0, \end{aligned} \tag{14}$$

where $\mathcal{L}_{\mathrm{coll}}(f^{(2)})$ incorporates binary collisions via a collision operator. We consider the inelastic collision operator eq. (11). Long range interactions are included in

$$\begin{aligned} \mathcal{L}_{\mathrm{part}}(f^{(2)}, f^{(3)}, ..., f^{(N)}) = \int_{\mathbb{R}^d} \int_{\mathbb{R}^d} \mathrm{d}\boldsymbol{r}_2 \, \mathrm{d}\boldsymbol{p}_2 \boldsymbol{\nabla}_{\boldsymbol{r}} v_2(\boldsymbol{r}, \boldsymbol{r}_2) \cdot \boldsymbol{\nabla}_{\boldsymbol{p}} f^{(2)} \\ - \int_{\mathbb{R}^{2d}} \int_{\mathbb{R}^{2d}} \mathrm{d}\boldsymbol{r}_2 \, \mathrm{d}\boldsymbol{p}_2 \, \mathrm{d}\boldsymbol{r}_3 \, \mathrm{d}\boldsymbol{p}_3 \boldsymbol{\nabla}_{\boldsymbol{r}} v_3(\boldsymbol{r}, \boldsymbol{r}_2, \boldsymbol{r}_3) \cdot \boldsymbol{\nabla}_{\boldsymbol{p}} f^{(3)} + ..., \end{aligned} \tag{15}$$

where, for example, $v_2(\boldsymbol{r}, \boldsymbol{r}_2)$ relates to the two-body potential $V_2(\boldsymbol{r}_i, \boldsymbol{r}_j)$, where the prefactor of $\frac{1}{2}$ has been absorbed by a symmetry argument.

2.3 DDFT Derivations

As the BBGKY equations are hierarchical, they do not constitute a small enough closed set of equations for efficient simulation. We therefore must truncate the hierarchy, and introduce additional assumptions to close the remaining set of equations.

Equation (14) involves integrals with higher order distribution functions which must be approximated. We consider moments of eq. (14), and close this system by approximating higher order moments and distributions using lower order counterparts. We first approximate the many-body interactions (eq. (15)) in the non-equilibrium fluid by those of an equilibrium fluid with the same one body density profile [3]:

$$\rho(\boldsymbol{r})\boldsymbol{\nabla}_{\boldsymbol{r}}\frac{\delta\mathcal{F}_{\text{ex}}[\rho(\boldsymbol{r})]}{\delta\rho(\boldsymbol{r})} = -\int_{\mathbb{R}^d}\mathrm{d}\boldsymbol{p}\mathcal{L}_{\text{part}}(f^{(2)}, f^{(3)}, ..., f^{(N)}), \tag{16}$$

where

$$\mathcal{F}[\rho] \coloneqq k_BT\int\mathrm{d}\boldsymbol{r}\rho(\boldsymbol{r})[\ln\Lambda^3\rho(\boldsymbol{r},t)-1]+\mathcal{F}_{\text{ex}}[\rho(\boldsymbol{r},t)]+\int\mathrm{d}\boldsymbol{r}V_{ext}(\boldsymbol{r})\rho(\boldsymbol{r},t), \tag{17}$$

is the Helmholtz free energy functional, with excess part $\mathcal{F}_{\text{ex}}[\rho(\boldsymbol{r})]$ [25], $\delta/\delta\rho(\boldsymbol{r})$ is a functional derivative, ad Λ is the (irrelevant) thermal De Broglie wavelength. We also assume that higher order distributions are uncorrelated in velocity:

$$f^{(k)}(\boldsymbol{r}^k,\boldsymbol{p}^k,t) = g^{(k)}(\boldsymbol{r}^k,\boldsymbol{p}^k,t)\prod_{i=1}^{k}f^{(1)}(\boldsymbol{r}_i,\boldsymbol{p}_i,t), \tag{18}$$

for $2 \leq k \leq N$, where $g^{(k)}$ is the k-correlation function. Of particular importance in our model is the pair correlation function for $k = 2$. To derive the continuum model discussed here, we must assume that $g^{(2)}$ does not depend on the particle velocities. We will discuss the validity of this assumption and the radial correlation function in more detail in section 2.4.

We note that, upon truncation of the hierarchy and approximation of higher order distributions in terms of low order counterparts, information from the Liouville equation (the N^{th} equation in the BBGKY hierarchy), in particular volume exclusion effects, are lost. It is therefore necessary to include a term which approximates volume exclusion from the Liouville equation. It is popular to include a pairwise interaction 'potential' which forbids overlap:

$$V_2(\boldsymbol{r}_1,\boldsymbol{r}_2,t) = \begin{cases}0, & \text{if } \|\boldsymbol{r}_1-\boldsymbol{r}_2\| > \sigma,\\ \infty, & \text{if } \|\boldsymbol{r}_1-\boldsymbol{r}_2\| \leq \sigma.\end{cases} \tag{19}$$

The Helmholtz free energy functional can be generalised to include volume exclusion due to hard particles via a suitable modification of $\mathcal{F}_{\text{ex}}$. In one dimension we use the exact functional for volume exclusion derived by Percus [55],

while Fundamental Measure Theory (FMT) is used to accurately approximate volume exclusion for spheres [52] for $d > 1$. However, neither the 'potential' in (19) nor FMT directly include the effect of collisions in the system, which must be included using a collision operator.

The collision operator is also an alternative way of including volume exclusion effects. In [39], in one dimension, volume exclusion effects are incorporated by approximating the correlation function $g^{(2)}$ in the inelastic collision operator using an analytic form:

$$g^{(2)}(r, r \pm \sigma) = \frac{1}{1 - \eta(r \pm \sigma/2)}, \tag{20}$$

where $\eta(x)$ is the local packing fraction. As the packing fraction approaches 1, the value of $g^(2)$ given by eq. (20) blows up and, in an analogous way to the Percus free energy in eq. (29), causes volume exclusion in the model.

However, the numerics in the present work show that this approximation is not accurate for dynamics with inelastic collisions, where, in particular, the value of the correlation function at contact increases for low local densities, rather than decreasing as in the elastic case: as a result DDFTs based on such approximations give poor results. In Section 3 we provide an example which shows that when the correlation function is approximated by experimental data and a volume exclusion free energy term is absent, the local density can exceed physical limits (see fig. 7).

Returning to the derivation of a continuum model, we define $\rho, \boldsymbol{v}$ and $\boldsymbol{E}$ as the number density, the local average velocity and the granular temperature of the system respectively:

$$\rho(\boldsymbol{r}, t) = \int_{\mathbb{R}^d} \mathrm{d}\boldsymbol{p} f^{(1)}(\boldsymbol{r}, \boldsymbol{p}, t), \quad \boldsymbol{v}(\boldsymbol{r}, t) = \frac{1}{\rho(\boldsymbol{r}, t)} \int_{\mathbb{R}^d} \mathrm{d}\boldsymbol{p} \frac{\boldsymbol{p}}{m} f^{(1)}(\boldsymbol{r}, \boldsymbol{p}, t),$$
$$\boldsymbol{E}(\boldsymbol{r}, t) = \int_{\mathbb{R}^d} \mathrm{d}\boldsymbol{p} \frac{\boldsymbol{p} \otimes \boldsymbol{p}}{m^2} f^{(1)}(\boldsymbol{r}, \boldsymbol{p}, t). \tag{21}$$

We finally assume that the one particle distribution function can be approximated by a local equilibrium Maxwell-Boltzmann distribution [24]:

$$f^{(1)}_{le}(\boldsymbol{r}, \boldsymbol{p}, t) = \frac{\rho(\boldsymbol{r}, t)}{|2\pi m k_B T \boldsymbol{E}(\boldsymbol{r}, t)|^{1/2}} \exp\left(- \frac{(\boldsymbol{p} - m\boldsymbol{v}(\boldsymbol{r}, t))^T \boldsymbol{E}(\boldsymbol{r}, t)^{-1} (\boldsymbol{p} - m\boldsymbol{v}(\boldsymbol{r}, t))}{2 m k_B T} \right), \tag{22}$$

where $|\boldsymbol{E}|$ is the determinant of the matrix $\boldsymbol{E}$. It is well known that the local equilibrium of a granular fluid is in fact not Maxwellian [8], and other approximations are a topic of current research [18]. However, the assumption eq. (22) allows us to write the second moment of $f^{(1)}(\boldsymbol{r}, \boldsymbol{p}, t)$ as a product of the density $\rho(\boldsymbol{r}, t)$ and local average velocity $\boldsymbol{v}(\boldsymbol{r}, t)$. We expect other functional forms of the local equilibrium can be implemented in the same manner, but to introduce the model we use eq. (22).

The continuity equation is then derived by integrating eq. (14) with respect to $\boldsymbol{p}$, under the assumptions stated:

$$\frac{\partial \rho}{\partial t} = -\boldsymbol{\nabla}_{\boldsymbol{r}} \cdot (\rho \boldsymbol{v}). \tag{23}$$

By multiplying eq. (14) by $\boldsymbol{p}$, then integrating with respect to $\boldsymbol{p}$, standard calculus results lead to the momentum equation [3], which now includes the granular temperature, and the first moment of the collision operator:

$$\frac{\partial \boldsymbol{v}}{\partial t} + \boldsymbol{v} \cdot \boldsymbol{\nabla}_{\boldsymbol{r}} \boldsymbol{v} + \gamma \boldsymbol{v} + \frac{k_B T}{m\rho} \boldsymbol{\nabla}_{\boldsymbol{r}} \cdot (\rho (\boldsymbol{E} - \boldsymbol{I})) + \frac{1}{m} \boldsymbol{\nabla}_{\boldsymbol{r}} \frac{\delta \mathcal{F}[\rho]}{\delta \rho} - \frac{1}{m\rho} \boldsymbol{\mathcal{M}}_1(\mathcal{L}_{\text{coll}}) = 0, \tag{24}$$

and also includes the Helmholtz free energy functional eq. (17). Finally, when considering the third moment by multiplying by $\boldsymbol{p} \otimes \boldsymbol{p}$ then integrating with respect to momentum, by using eq. (24) and eq. (23), we arrive at an equation describing the evolution of the granular temperature:

$$\partial_t \boldsymbol{E} + \boldsymbol{v} \cdot \boldsymbol{\nabla}_{\boldsymbol{r}} \boldsymbol{E} + (\boldsymbol{E} \boldsymbol{\nabla}_{\boldsymbol{r}} \boldsymbol{v}) + (\boldsymbol{E} \boldsymbol{\nabla} \boldsymbol{v})^T + 2\gamma(\boldsymbol{E} - \boldsymbol{I}) - \frac{1}{k_B T \rho} \boldsymbol{\mathcal{M}}_2(\mathcal{L}_{\text{coll}}) = 0. \tag{25}$$

Equations (24) and (25) include centred moments of the collision operator:

$$\boldsymbol{\mathcal{M}}_1(\mathcal{L}_{\text{coll}}) = \int_{\mathbb{R}^d} \mathrm{d}\boldsymbol{p} \frac{(\boldsymbol{p} - \bar{\boldsymbol{p}})}{m} \mathcal{L}_{\text{coll}}(f^{(1)}, g^{(2)}), \tag{26}$$

$$\boldsymbol{\mathcal{M}}_2(\mathcal{L}_{\text{coll}}) = \int_{\mathbb{R}^d} \mathrm{d}\boldsymbol{p} \frac{(\boldsymbol{p} - \bar{\boldsymbol{p}}) \otimes (\boldsymbol{p} - \bar{\boldsymbol{p}})}{m^2} \mathcal{L}_{\text{coll}}(f^{(1)}, g^{(2)}), \tag{27}$$

where the argument of $\mathcal{L}_{\text{coll}}$ has changed to account for the assumption eq. (18). For eq. (11), by applying eq. (22), we can write eqs. (26) and (27) in terms of Gaussians and error functions. The exact forms used in simulations are given in appendix A.

Given the centred moments of $\mathcal{L}_{\text{coll}}(f^{(1)}, g^{(2)})$, and the correlations $g^{(k)}$, the set of equations eqs. (23) to (25) then constitute a closed model for granular media, incorporating volume exclusion due to hard particles, external and inter-particle potentials, and (in)elastic collisions.

There are some important differences between the DDFT model here and existing DDFTs in the literature. Firstly, we include moments of the collision operator eqs. (26) and (27), which must be included to incorporate dissipative effects due to inelastic collisions. Our numerical experiments (see fig. 3a) show that the collision terms do affect the dynamics, and that the effect is pivotal when $\alpha < 1$. We also include an additional moment eq. (25) of eq. (14), as the effects of the collision term are evident in the granular temperature of the system; eq. (4) reduces the variance of particle velocities when $\alpha < 1$, so

we expect it to have a dissipative effect on $\boldsymbol{E}(\boldsymbol{r}, t)$. In particular under our assumptions, in one dimension,

$$\lim_{\sigma\to 0} \boldsymbol{\mathcal{M}}_1(\mathcal{L}_{\text{coll}}) = 0, \quad \lim_{\sigma\to 0} \boldsymbol{\mathcal{M}}_2(\mathcal{L}_{\text{coll}}) = -\frac{2g^{(2)}(r)\rho^2(mk_BTE)^{3/2}(1-\alpha^2)}{\sqrt{\pi}}. \tag{28}$$

Thus inelasticity has a small effect on eq. (24), but can be incorporated by including an additional moment.

Although DDFT derivations involving collision terms [39] and temperature gradients [58] have been studied, it is clear that for granular media both terms play important roles. When comparing to results in kinetic theory, the addition of the free energy term allows us to include effects both from interparticle interactions and volume exclusion, by considering the interactions at the particle level.

We also note the importance in the choice of initial condition; the initial density, velocity and granular temperature must satisfy the physical restrictions of the PDE; in one dimension this corresponds to not exceeding the packing fraction limit $\rho_v = 1$, and that the density must be non-negative $\rho(r) \geq 0$ for all r.

In one dimension, we can incorporate volume exclusion exactly using the Percus free energy [45]:

$$\frac{\delta \mathcal{F}_{\text{ex}}[\rho]}{\delta \rho}(x) = \log\left(1 - \int_x^{x+\sigma} \rho(x')\,\mathrm{d}x'\right) + \int_{x-\sigma}^{x} \frac{\rho(x'')}{1 - \int_{x''}^{x''+\sigma} \rho(x')\,\mathrm{d}x'}\,\mathrm{d}x'' \tag{29}$$

We note that in one dimension for constant ρ, as $\rho \to \frac{1}{\sigma}$, we approach the maximum density and so $\frac{\delta \mathcal{F}_{\text{ex}}[\rho]}{\delta \rho} \to \infty$, *i.e.* the chemical potential of the system blows up. This can be seen as a constraint on adding particles to the system, and implicitly stops the volume of the system increasing beyond the physical limit; eq. (29) is defined so that it is limited by the close packing value. These effects are not present when solely including a collision operator with arbitrary g, such as those obtained from microscopic simulations.

2.4 Approximating the pair correlation function

Equations (23)-(25) as they are written do not constitute a closed continuum model, as the Helmholtz free energy functional (in particular the parts that involve interaction potentials) and the inelastic collision operator both depend on the pair correlation function $g^{(2)}(\boldsymbol{r}^2, \boldsymbol{p}^2, t)$.

In principle $g^{(2)}$ explicitly depends on all of its arguments. In particular, it is known that when modelling systems of hard spheres as a fluid, velocity correlations have strong effects on structures within non-equilibrium systems [35]. These velocity correlations have been well-studied for granular fluids [36] at the atomic scale. To improve the model considered here one should account

for these results in the derivation of the DDFT, and in the pair correlation function.

In some models, and particular in popular DDFT models [23,3], $g^{(2)}$ is assumed to be independent of $\boldsymbol{v}_1$ and $\boldsymbol{v}_2$. For systems with soft particles where interparticle potentials are independent of velocity, this is generally seen to be an accurate assumption. Furthermore, for systems where particles interact with radial potentials (such as systems of hard spheres), $g^{(2)}$ is also assumed to be radially symmetric, *i.e.* $g^{(2)} = g^{(2)}(\|\boldsymbol{r}_1 - \boldsymbol{r}_2\|, t)$. By assuming that $g^{(2)}$ is independent of velocity we have also simplified the derivation of eqs. (23) to (25), at the penalty of reducing the accuracy of the model, which we will discuss in more details in section 3.

Obtaining a time-dependent approximation of $g^{(2)}$ is also challenging. In [28], by using maximum entropy closure methods, a closed set of equations for soft particles is constructed, which includes a partial differential equation that describes the evolution of $g^{(2)}$. However, the resulting equations have six spatial dimensions, which makes them highly challenging to simulate efficiently. Furthermore, the maximum entropy assumptions are not necessarily valid for granular fluids. Analytical approaches to finding $g^{(2)}$ are also generally restricted to simple systems [30].

As a result it is also common to approximate the radial correlation function at some steady state. It is known [49] that higher order correlations equilibriate much faster than the density. This result validates the *adiabatic approximation*; correlations can be approximated by their local equilibrium values. When considering systems of hard, elastic spheres the local equilibrium value for the pair correlation function can be obtained efficiently using particle simulation methods, by simulating the dynamics until the mean-free path equilibrates, then measuring relative particle positions. In [45], in one dimension, the radial correlation function is approximated by this equilibrium form eq. (20). However, due to clustering effects between inelastic hard spheres, this approximation is no longer accurate for granular fluids. In this case, many authors use the *homogeneous cooling state* [9], which can be constructed empirically by running particle simulations until the granular temperature is close to zero. The result is independent of α when $\alpha < 1$, which will not be useful here as all resulting dynamics will look the same.

In our simulations, we choose to approximate $g^{(2)}$ locally by simulating a small collection of particles over shorter times than it takes to reach the homogeneous cooling state. Our justification is as follows: In systems of particles outside of equilibrium, the system will never reach a point where the homogeneous cooling state is valid. At the timescales of interest it is therefore more appropriate to take an approximation of $g^{(2)}$ that is constructed at the same timescale. We use viscous drag to determine a natural timescale for the system: we simulate small systems of particles until 99% of the kinetic energy of the system has dissipated. This is a shorter time than is considered in the homogeneous cooling state: and is a relatively short time in out simulations, as the kinetic energy dissipates exponentially due to viscous drag. There are

of course many other ways that an appropriate timescale can be determined, and in practice this should depend on the system of interest.

The resulting values for $g^{(2)}$ are parametrised by the local density ρ (as a result of considering small collections of particles) and the coefficient of restitution α. In this work we will only consider one value for γ, but a similar study could consider how the strength of viscous drag effects the pair correlation function.

By applying statistical methods on synthetic data generated by extensive particle simulations with small N, we parametrise $g^{(2)}$ without simulating the entire system, avoiding excessive computational cost. We can then incorporate it in the model eqs. (23) to (25). Analogously, parametrisations could (and should, if possible) be performed with experimental data.

3 Numerical results

3.1 Parametrisation of $g^{(2)}(\sigma)$

We present an example of our methodology for constructing $g^{(2)}$ using a system of 100 deterministic hard rods ($d = 1$) on a 2π-periodic domain in the absence of external or interparticle potentials, with $\gamma = 2$ and $\sigma = 2\pi/25,000$. In the absence of a thermostat, the trajectories of individual particles can then be solved analytically. Therefore, instead of a numerical method involving a timestep for microscopic simulation, we predict collision times of particles, then sort and schedule and process these events before advancing simulation. This methodology is at the centre of Event Driven Particle Dynamics (EDPD), which was first developed as early as the 1950s [2], but is still a modern topic of research [6].

A naïve EDPD algorithm will predict future collisions between all particles after each collision has been processed, producing an algorithm with computational complexity $O(N^2)$ per collision. Our simulations use the cell method [1] to reduce the computational cost of event prediction to $O(N)$. We also update the position of each particle asynchronously [32], which reduces the cost of advancing simulation to $O(1)$. In addition, data structures such as binary search trees [47] and bounded increasing priority queues [44] can be implemented to decrease the computational cost of event sorting and scheduling to $O(1)$ per collision. Combining methods for prediction and scheduling gives dynamics with a cost of $O(1)$ per collision. Software packages such as `DynamO` [7] implement all of these methods, but are currently limited to systems with friction coefficient $\gamma = 0$. Finally, methods to efficiently parallelise EDPD algorithms have also been constructed [26].

In addition, several numerical methods are available to avoid inelastic collapse in EDPD. A review of these methods is available in [33], and in our simulations, we implement the TC model, which renders collisions elastic when a pair of particles undergo a collision a small time $t_c > 0$ after their previous collision. The precise value of t_c can be determined by the other timescales

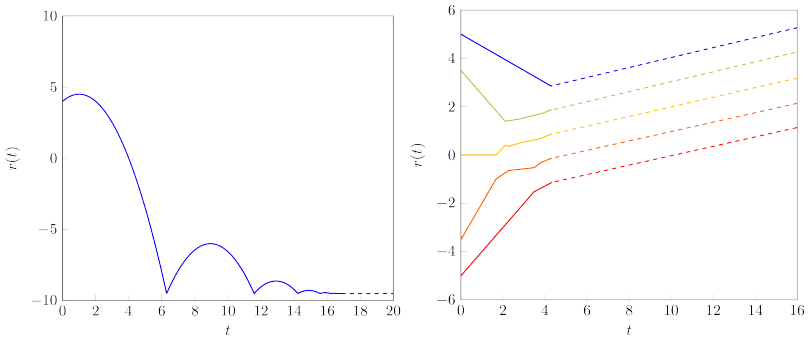

(a) (b)

Fig. 1: EDPD simulations displaying inelastic collapse in one dimension. Left: A single inelastic particle with $\alpha = 0.8$ under the effect of gravity in a domain with hard walls. Right: A collection of inelastic particles with $\alpha = 0.5$ in a periodic domain. The solid lines and dashed lines show the same number of collisions, where the TC method has been implemented for the dashed lines with $t_c = 10^{-5}$, allowing dynamics to advance.

of the system: for example t_c can be taken as a small fraction of the mean-free path in a system of elastic particles, for use in the inelastic counterpart. Together with polydispersity, the TC method stops sharp peaks from forming in the radial correlation function, but also accurately approximates the dynamics of the system. We give two examples of situations that undergo inelastic collapse in one dimension in fig. 1. When $\alpha < 1$, an infinite number of collisions occurs in finite time, so the dynamics are 'jammed'. The TC model allows the particle to 'vibrate' when the collisions become very frequent. A collision between two particles is rendered elastic only when colliding particle velocities are very similar, thus the application of the TC method should not significantly alter the global outcome of the dynamics, unless especially long timescales are considered. We note that, by design, volume exclusion is incorporated in the algorithm; collisions are predicted and processed so that particles do not overlap. Therefore unlike in continuum modelling, we do not require any additional potential in these dynamics to include volume exclusion effects.

Using EDPD to construct 5000 samples of each system with a range of values of α and solid volume fractions ρ_v, we construct a parametrisation of $g^{(2)}(\sigma)$ that is appropriate for the system of interest. Examples of systems with $\alpha = 0.9$ and $\alpha = 0.5$ are given in fig. 2. We see that particle streaming is more evident at earlier times when α is smaller. We note that over long times in a system where $\gamma = 0$ and the particle velocities are centred at 0, inelastic one-dimensional particles will eventually reach the homogeneous cooling state [9], forming large clusters of streaming particles.

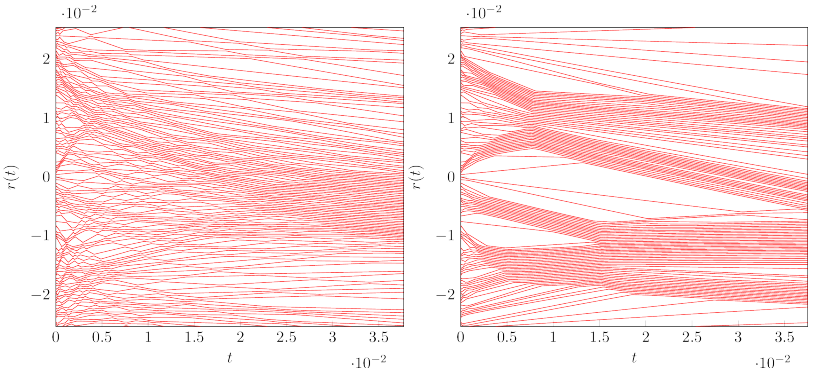

(a) (b)

Fig. 2: Samples that can be used to construct $g^{(2)}(\sigma)$ at different points in time. The red lines are trajectories of the centres of mass of individual particles. We note that the domain is periodic, so trajectories can disappear and reappear at the top and bottom of the y axis. Left: $\alpha = 0.9$, right: $\alpha = 0.5$. In these examples the initial conditions are the same, but display characteristic differences in their dynamics, in particular when $\alpha = 0.5$ particle streaming is more evident.

However when $\gamma > 0$ the homogeneous cooling state will not be reached: the viscous drag present in the system will reduce the velocities of some particles before they have a chance to collide. This also implies that the size of clusters in systems that include viscous drag will be smaller and more uniform than in systems where $\gamma = 0$, which allows us to use smaller systems of particles to construct reasonable continuum parameters for DDFT simulations.

For $d = 1$ in the absence of friction, external and interparticle potentials, the radial correlation function blows up when particles are monodisperse and inelastic; at equilibrium all particles will be moving in contact. We therefore include a variance in the diameter of particles $\sigma_v = 0.1\sigma$. Equations (23) to (25) can be adapted to take into account poly-dispersity, but we expect the effect to be negligible in this case and so we ignore it in the DDFT. In each sample, the initial velocities of the particles are normally distributed with mean 0 and variance 1, and positions are drawn from a uniform distribution in the domain. We evolve the system until 99.9% of the energy of the particles has dissipated due to inelasticity and friction, then construct a near equilibrium parametrisation of $g^{(2)}(\|r_1 - r_2\|)$. We note that when ρ_v is small and α is close to 1, few collisions happen before the effect of friction causes particles to lose all their energy, and when $\rho_v = 1$, the system is fully dense, so the value of the correlation function is independent of α.

In fig. 3a, we display $g^{(2)}(\|r_1 - r_2\|)$ for different densities, as well as g at time $t = 0$. We note that for low densities and $\alpha = 0.5$ the radial correlation function has several peaks. This is evidence of particle streaming, where

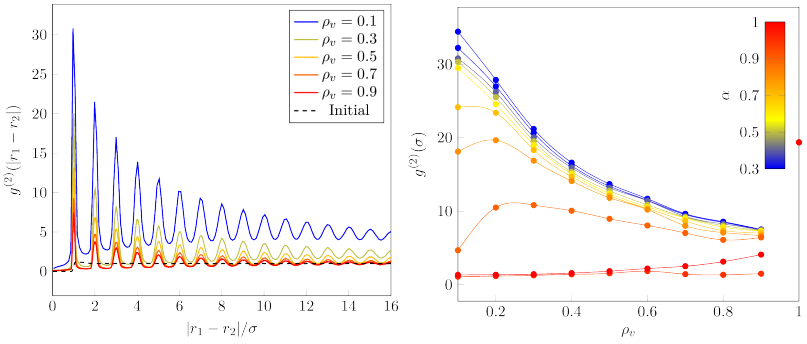

(a) (b)

Fig. 3: Left: the radial correlation function $g^{(2)}(\|r_1 - r_2\|)$ for $\alpha = 0.5$, with different solid fractions ρ_v. Right: cubic spline interpolation of $g^{(2)}(\sigma)$ varying over ρ_v, for different values of α.

inelastic collisions cause particles to move at the same velocity, near to one another.

Under the assumption that $g^{(2)} = g^{(2)}(\|r_1 - r_2\|)$, only the value of $g^{(2)}$ at $\|r_1 - r_2\| = \sigma$ is included in the collision terms. In fig. 3b we use the results of particle simulations to parametrise $g^{(2)}(\sigma)$ for different α and ρ_v, using cubic smoothing spline interpolation [12]. We omit the point when $\sigma_v = 1$ from the interpolation to improve the curve fit for values used in the DDFT simulation.

3.2 Example

To test the validity of the continuum model, and the effects of our assumptions, we will consider a one dimensional, periodic example. We consider a periodic domain $[0, 100]$. To match the simulations used to parametrise $g^{(2)}$, we will set $\gamma = 2$ and $\sigma = 2\pi/25,000$, so that there are $120,000$ particles in the system (a fully packed domain would hold $400,000$ particles in this case). In this case we will not be able to simulate the microscopic dynamics as the number of events that occurs in the time frame of interest is computationally intractable. For particle simulations we consider systems with roughly 240 particles, that result in the same density and other dimensionless values as a comparative continuum simulation.

Before continuing, we note that the system can be made dimensionless by considering the following scaling:

$$\gamma \sim \frac{1}{T}, \quad k_B T \sim \frac{L^2 M}{T^2}, \quad \rho \sim \frac{1}{L}, \quad v \sim \frac{L}{T}, \quad m \sim M, \tag{30}$$

where L is a length scale (in our simulations we use the domain length, but the particle diameter could also be considered), T is a time scale and M is

a mass scale (the mass of a particle). Furthermore, the granular temperature is dimensionless. The scaling of variables and parameters are constructed by considering the the microscopic dynamics and the distributions $f^{(N)}$ as in [39].

The initial conditions are given by

$$\rho_0(r) = \frac{\rho_v}{N_c}\left(e^{\frac{(r-25)^2}{25}} + e^{\frac{(r-75)^2}{25}} + 0.5\right), \quad v_0(r) = 20\sin\left(\frac{2\pi r}{100}\right), \quad E_0(r) = E_0, \tag{31}$$

where N_c is a normalisation constant, and $\rho_v = 0.3$ is the total solid volume fraction, and we choose different values for $E_0 > 0$. The initial conditions are chosen such that areas of higher density will move toward one another and 'collide'.

3.2.1 Microscopic simulation

We produce 200 samples of initial conditions, by using a slice-sampling method [42] to ensures that particles are not overlapping at time $t = 0$, and that the initial density is similar to $\rho_0(r)$. The initial velocities are also sampled from a Maxwellian with position-dependent mean $v_0(r)$ and variance E_0. We run all dynamics until the particles come to rest, which occurs for most samples at around $t = 5$, independent of the choice of α or E_0.

In fig. 4 we present the effect of different values of E_0 on the dynamics of the system. The curves shown are produced using kernel density estimates [14] of the sample positions. The inaccuracies in the densities at the edges of the domain are due to numerical errors in the kernel density estimate and should be ignored. We note that there are differences in the evolution of the peaks in the density when $E_0 = 100$, in particular in the initial stages of the simulation. In fig. 5 we set $E_0 = 250$ (to match the continuum simulations) and consider the effect of different values of α. We note that there is a large difference between the elastic ($\alpha = 1$) and inelastic case ($\alpha < 1$): in the inelastic case the peaks remain in the simulation, as particle collisions dissipate granular temperature at a faster rate than in the elastic case. There are also differences in the shape of the peaks for different inelastic choices of α, where energy is dissipated at different rates.

3.2.2 DDFT Simulation

For a continuum approach we simulate eqs. (23) to (25). We use pseudospectral code provided in [43], which is available at [22]. Across the periodic domain we use 100 equally spaced computational points. Using more than 100 points has little effect on the result of the simulation. We include the Percus free energy functional [45] to incorporate volume exclusion in the dynamics.

Figure 6 displays results of model eqs. (23) to (25) at different times t when $\alpha = 0.5$. The results show that every term is necessary for accurate dynamics: If the Percus term is neglected the density is sometimes overestimated as particle

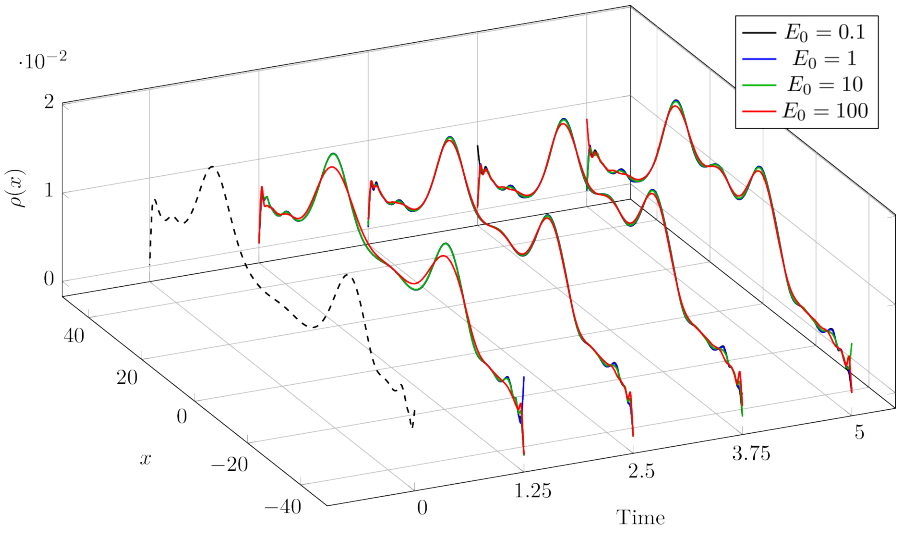

Fig. 4: Results from microscopic simulations for $\alpha = 0.5$. The kernel density estimate of the initial condition for all simulations (black, dashed) is displayed at time 0.

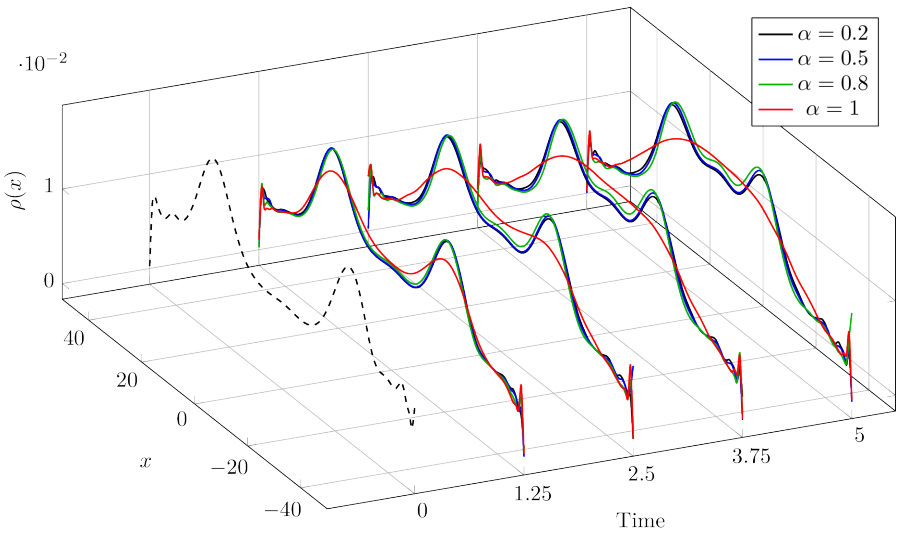

Fig. 5: Results from microscopic simulations for $E_0 = 250$. Each the initial condition for all simulations (black, dashed) is displayed at time 0.

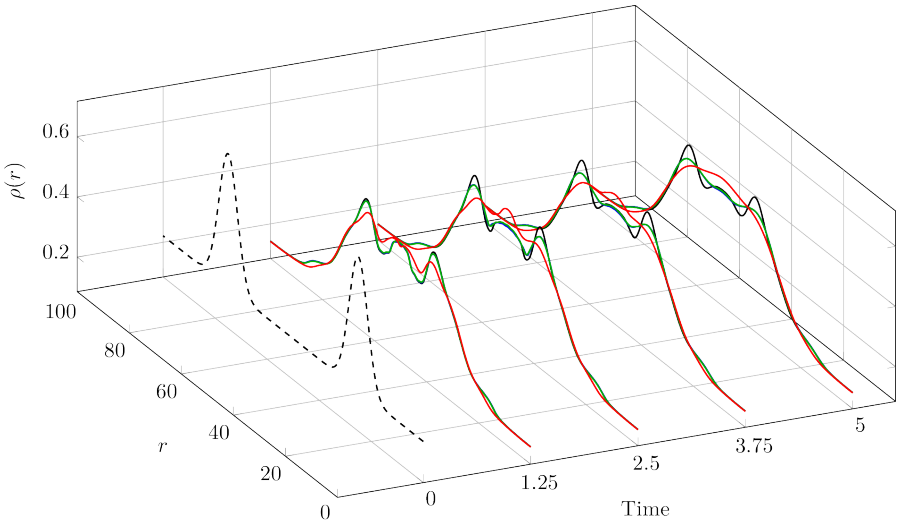

Fig. 6: Results from the DDFT simulation for $\alpha = 0.5$. Each simulation has the same initial condition (black, dashed) at time 0. The black line neglects the collision operator and the free energy term. The blue line includes the free energy term but not the collision operator. The green line includes both terms, with $g^{(2)}(\sigma) = 1$, and the red line includes both terms and uses $g^{(2)}(\sigma)$ determined by particle simulations, shown in fig. 3b.

volume exclusion of hard particles is not incorporated. If the collision term is included but $g^{(2)}(\sigma) = 1$ (i.e. the uncorrelated case) the inelastic effects are not noticeable, and the high density areas are reflected upon 'collision'. When all terms are present with $g^{(2)}$ constructed from particle simulations we see that the two higher density areas coalesce, an intuitive result for inelastic dynamics.

To show the importance of including a volume exclusion free energy term in the DDFT, we consider an example with modified initial conditions: we set $N = 175,000$, and

$$v_0(r) = 26 \sin\left(\frac{2\pi r}{100}\right). \tag{32}$$

The results in fig. 7 show that the system reached an unphysical density in finite time if the Percus free energy is not included.

Finally, we perform the same dynamics for different α with initial conditions eq. (31). The results in fig. 8 show that particles coalesce more for smaller α. In fig. 9 we provide the density near equilibrium for different coefficients of restitution. We note that in this example, the long time behaviour of the density is similar for all coefficients of restitution. This is because the effect of the collision operator is small when the local average velocity is small, so in

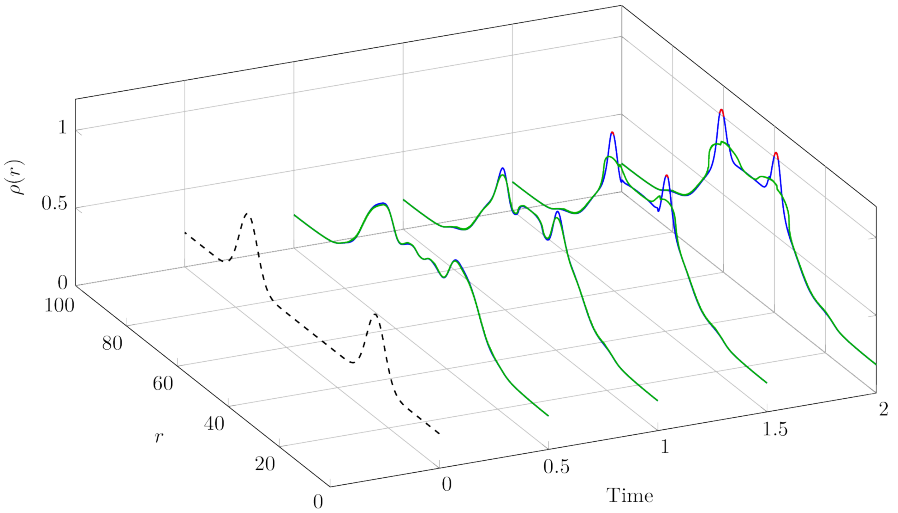

Fig. 7: Results from the DDFT simulation, using $g^{(2)}(\sigma)$ determined by particle simulations for $\alpha = 1$, and the same initial condition (black, dashed). The blue line gives the result when the free energy term is neglected, and the green is the same simulation with the Percus free energy term included. Any values of ρ which are above the physical limit of $\rho = 1$ are coloured red. In this example we used 600 computational points, to ensure that the volume exclusion effects are numerically stable.

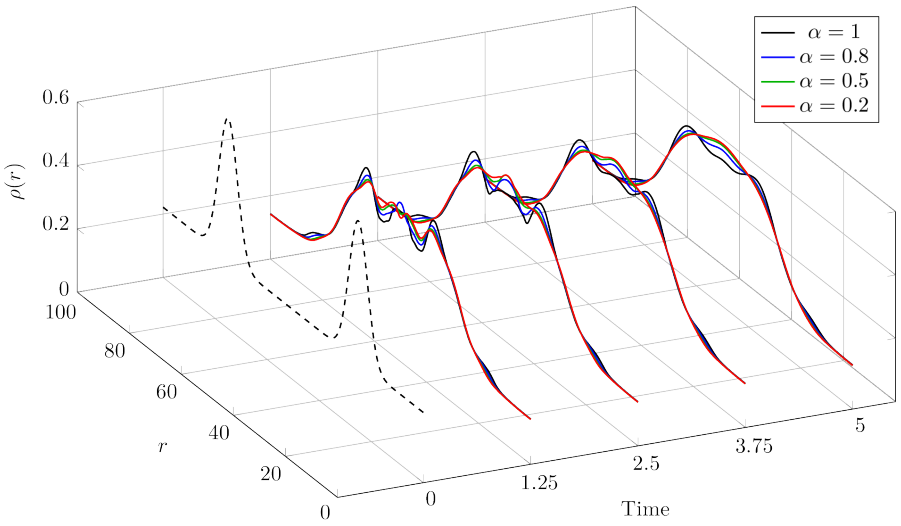

Fig. 8: Results from the DDFT simulation, using $g^{(2)}(\sigma)$ determined by particle simulations for different α, using the same initial condition (black, dashed).

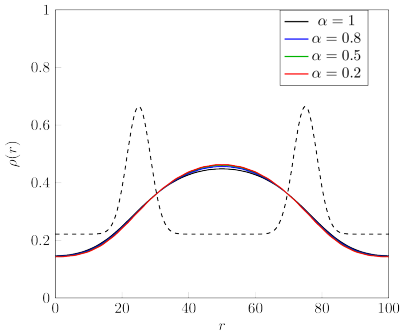

Fig. 9: The density at time $T = 50$ for different coefficients of restitution, compared to the initial density (black, dashed).

this example where energy is not added into the system using any other external potentials, the effect of friction determines the dynamics for long times. This phenomena is not observed in the microscopic simulations where the is no thermostat driving the dynamics once kinetic energy has dissipated due to collisions and viscous drag.

We note that the DDFT results are numerically stable for the choice of parameters, however there are clear qualitative differences in the particle and continuum cases. This may be due to the scale of the particle systems considered: there is some evidence [20] to show that $\mathcal{O}(10^5)$ particles are required in a particle system to achieve a good agreement with DDFTs, in simpler particle systems where there are no particle collisions or inertial effects. However, in other cases DDFT models agree reasonably well with particle simulations for systems of hundreds of particles [23].

Our results show that neglecting velocity correlations and assuming a Maxwellian local equilibrium (assumptions which are also present in many popular DDFT models) removes key physical properties of the granular fluid.. The results discussed here can then be used to determine which systems DDFT models can be reliably applied to, and will guide future derivations and DDFT models.

4 Conclusions and future work

We have constructed a new model for granular media, which can incorporate inelastic collisions using classical collision operators, and interparticle interactions using DDFT methods. We have presented a simple example which displays the importance of each term in the model, but the model can also be used for systems in 2D or 3D with more complicated dynamics such as adhesion between particles. This is, as far as we know, the first attempt at validating a DDFT for granular media, and so is an important contribution to guide further research on the topic.

Our results show that our methodology is successful; small scale, inexpensive particle dynamics can be used to fine-tune parameters in the mesoscopic model, such as the radial correlation function. However, the applications of the model are currently limited in scope, due to the assumptions applied at the end of the DDFT derivation. The effectiveness of the model should improve upon relaxation of the assumptions in the derivation, for example by removing the Maxwellian local equilibrium distribution and by producing a more intricate parametrisation of the radial correlation function. In particular, we believe that the accuracy of the model can be dramatically improved by careful consideration of the velocity correlations in the system, in an analogous way to that discussed in [35].

Much of the current research on DDFT for complex fluids can also be adapted to the system of equations in this work, including extension to polydisperse or multi-species systems [21], and inclusion of more complicated drag forces due to interactions between the particles and fluid in the system using a hydrodynamic interaction tensor [23]. Further work on fundamental derivations in the style of [57,29] will be beneficial to construct collision operators from more complicated dynamics or particles. Furthermore, inclusion of a more accurate local (non-Maxwellian) equilibrium approximation for granular media could improve the model.

The synthetic data presented is an example of how modern computational and data-scientific methods can be applied to fine-tune parameters in continuum models; we parametrise using statistics from particle simulations. For systems with more complicated interactions between particles we will need to use state of the art particle simulation methods, but our modelling approach avoids the computational bottleneck caused by simulating large numbers of particles.

4.1 Acknowledgements

TDH was supported by The Maxwell Institute Graduate School in Analysis and its Applications, a Centre for Doctoral Training funded by the UK EPSRC (EP/L016508/01), the Scottish Funding Council, Heriot-Watt University and the University of Edinburgh. RO and BDG acknowledge the support of EPSRC (EP/N034066/1 and EP/L025159/1, respectively). The authors would like to acknowledge helpful discussions with Dr. M. Wilkinson (Nottingham Trent University).

References

1. Alder, B.J., Wainwright, T.E.: Phase transition for a hard sphere system. The Journal of chemical physics **27**(5), 1208–1209 (1957)
2. Alder, B.J., Wainwright, T.E.: Studies in molecular dynamics. i. general method. The Journal of Chemical Physics **31**(2), 459–466 (1959)

3. Archer, A.J.: Dynamical density functional theory for molecular and colloidal fluids: a microscopic approach to fluid mechanics. J. Chem. Phys. **130**, 014509 (2009). DOI 10.1063/1.3054633
4. Bagnold, R.A.: The physics of blown sand and desert dunes. Dover Earth Science. Dover Publications (2005). URL https://books.google.co.uk/books?id=gKAoAwAAQBAJ
5. Balescu, R.: Equilibrium and nonequilibrium statistical mechanics. NASA STI/Recon Technical Report A **76**, 756 (1975)
6. Bannerman, M.N., Green, T.E., Grassia, P., Lue, L.: Collision statistics in sheared inelastic hard spheres. Phys. Rev. E. **79**(4), 041308 (2009)
7. Bannerman, M.N., Sargant, R., Lue, L.: Dynamo: a free $\mathcal{O}(N)$ general event-driven molecular dynamics simulator. J. Comput. Chem. **32**(15), 3329–3338 (2011)
8. Benedetto, D., Caglioti, E., Carrillo, J.A., Pulvirenti, M.: A non-Maxwellian steady distribution for one-dimensional granular media. J. Stat. Phys. **91**(5-6), 979–990 (1998)
9. Brilliantov, N.V., Pöschel, T.: Kinetic theory of granular gases. Oxford University Press (2010)
10. Brown, R.: A brief account of microscopical observations made in the months of June, July and August 1827, on the particles contained in the pollen of plants; and on the general existence of active molecules in organic and inorganic bodies. Philos. Mag. **4**(21), 161–173 (1828). DOI 10.1080/14786442808674769
11. Chan, G.K., Finken, R.: Time-dependent density functional theory of classical fluids. Phys. Rev. Lett. **94**, 183001 (2005). DOI 10.1103/PhysRevLett.94.183001. URL https://link.aps.org/doi/10.1103/PhysRevLett.94.183001
12. Craven, P., Wahba, G.: Smoothing noisy data with spline functions. Numer. Math. **31**(4), 377–403 (1978)
13. Cundall, P.A., Strack, O.D.L.: A discrete numerical model for granular assemblies. Geotechnique **29**(1), 47–65 (1979)
14. Davis, R.A., Lii, K.S., Politis, D.N.: Remarks on some nonparametric estimates of a density function. In: Selected Works of Murray Rosenblatt, pp. 95–100. Springer (2011)
15. Durán-Olivencia, M.A., Goddard, B.D., Kalliadasis, S.: Dynamical density functional theory for orientable colloids including inertia and hydrodynamic interactions. Journal of Statistical Physics **164**(4), 785–809 (2016)
16. Einstein, A.: Über die von der molekularkinetischen theorie der wärme geforderte bewegung von in ruhenden flüssigkeiten suspendierten teilchen. Ann. Phys. **322**(8), 549–560 (1905). DOI 10.1002/andp.19053220806. URL http://dx.doi.org/10.1002/andp.19053220806
17. Ermak, L.E., McCammon, J.A.: Brownian dynamics with hydrodynamic interactions. J. Chem. Phys. **69**(4), 1352–1360 (1978). DOI 10.1063/1.436761
18. Garzó, V., Hrenya, C.M., Dufty, J.W.: Enskog theory for polydisperse granular mixtures. ii. sonine polynomial approximation. Phys. Rev. E. **76**(3), 031304 (2007)
19. Gidaspow, D.: Multiphase flow and fluidization: continuum and kinetic theory descriptions. Academic press (1994)
20. Goddard, B.D., Gooding, B., Pavliotis, G.A., Short, H.: Noisy bounded confidence models for opinion dynamics: the effect of boundary conditions on phase transitions (2020)
21. Goddard, B.D., Nold, A., Kalliadasis, S.: Multi-species dynamical density functional theory. J. Chem. Phys. **138**(14), 144904 (2013)
22. Goddard, B.D., Nold, A., Kalliadasis, S.: 2DChebClass [Software]. http://dx.doi.org/10.7488/ds/1991 (2017)
23. Goddard, B.D., Nold, A., Savva, N., Pavliotis, G.A., Kalliadasis, S.: General dynamical density functional theory for classical fluids. Phys. Rev. Lett. **109**(12), 1–5 (2012). DOI 10.1103/PhysRevLett.109.120603
24. Hansen, J., McDonald, I.R.: Theory of simple liquids. Elsevier (1990)
25. Henderson, D.: Fundamentals of inhomogeneous fluids. CRC Press (1992)
26. Herbordt, M.C., Khan, M.A., Dean, T.: Parallel discrete event simulation of molecular dynamics through event-based decomposition. 2009 20th IEEE International Conference on Application-specific Systems, Architectures and Processors pp. 129–136 (2009). DOI 10.1109/ASAP.2009.39
27. Huang, K.: Statistical mechanics. Wiley (1987). URL https://books.google.co.uk/books?id=M8PvAAAAMAAJ

28. Hughes, K.H., Burghardt, I.: Maximum-entropy closure of hydrodynamic moment hierarchies including correlations. J. Chem. Phys. **136**(21), 214109 (2012)
29. Hurst, T.D., Goddard, B.D., Wilkinson, M.: A derivation of the liouville equation for hard particle dynamics with non-conservative interactions. P. Roy. Soc. Edinb. A p. to appear (2020)
30. Ibsen, J., Cordero, P., Tabensky, R.: Hard rods in the presence of a uniform external field. J. Chem Phys. **107**(14), 5515–5523 (1997)
31. Louge, M.: The surprising relevance of a continuum description to granular clusters. Journal of Fluid Mechanics **742**, 1–4 (2014)
32. Lubachevsky, B.D.: How to simulate billiards and similar systems. Journal of Computational Physics **94**(2), 255–283 (1991)
33. Luding, S., McNamara, S.: How to handle the inelastic collapse of a dissipative hard-sphere gas with the TC model. Granul. Matter **1**(3), 113–128 (1998). DOI 10.1007/s100350050017
34. Lun, C.K.K., Savage, S.B., Jeffrey, D.J., Chepurniy, N.: Kinetic theories for granular flow: inelastic particles in Couette flow and slightly inelastic particles in a general flow-field. J. Fluid Mech. **140**, 223–256 (1984)
35. Lutsko, J.F.: Velocity correlations and the structure of nonequilibrium hard-core fluids. Physical review letters **86**(15), 3344 (2001)
36. Lutsko, J.F.: Atomic-scale structure of hard-core fluids under shear flow. Physical Review E **66**(5), 051109 (2002)
37. Lutsko, J.F.: Recent developments in classical density functional theory. Adv. Chem. Phys. **144**, 1–92 (2010)
38. Marconi, U., Tarazona, P.: Dynamic density functional theory of fluids. J. Chem. Phys. **110**(16), 8032–8044 (1999)
39. Marconi, U., Tarazona, P., Cecconi, F.: Theory of thermostatted inhomogeneous granular fluids: A self-consistent density functional description. J Chem. Phys. **126**(16), 1–13 (2007). DOI 10.1063/1.2723744
40. McNamara, S., Young, W.: Inelastic collapse in two dimensions. Physical review. E, Statistical physics, plasmas, fluids, and related interdisciplinary topics **50**, R28–R31 (1994). DOI 10.1103/PhysRevE.50.R28
41. Mitrano, P.P., Zenk, J.R., Benyahia, S., Galvin, J.E., Dahl, S.R., Hrenya, C.M.: Kinetic-theory predictions of clustering instabilities in granular flows: beyond the small-knudsen-number regime. Journal of Fluid Mechanics **738**, R2 (2014). DOI 10.1017/jfm.2013.602
42. Neal, R.M.: Slice sampling. Annals of statistics pp. 705–741 (2003)
43. Nold, A., Goddard, B.D., Yatsyshin, P., Savva, N., Kalliadasis, S.: Pseudospectral methods for density functional theory in bounded and unbounded domains. J. Comput. Phys. **334**, 639–664 (2017)
44. Paul, G.: A complexity $\mathcal{O}(1)$ priority queue for event driven molecular dynamics simulations. J. Comput. Phys. **221**(2), 615–625 (2007). DOI 10.1016/j.jcp.2006.06.042
45. Percus, J.K.: Equilibrium state of a classical fluid of hard rods in an external field. J. Stat. Phys. **15**(6), 505–511 (1976). DOI 10.1007/BF01020803. URL https://doi.org/10.1007/BF01020803
46. Queteschiner, D., Lichtenegger, T., Pirker, S., Schneiderbauer, S.: Multi-level coarse-grain model of the dem. Powder Technology **338**, 614–624 (2018)
47. Rapaport, D.: The event scheduling problem in molecular dynamic simulation. Journal of Computational Physics **34**(2), 184 – 201 (1980). DOI https://doi.org/10.1016/0021-9991(80)90104-7. URL http://www.sciencedirect.com/science/article/pii/0021999180901047
48. Rauchenzauner, S., Schneiderbauer, S.: A dynamic anisotropic spatially-averaged two-fluid model for moderately dense gas-particle flows. International Journal of Multiphase Flow p. 103237 (2020)
49. Rex, M., Löwen, H.: Dynamical density functional theory for colloidal dispersions including hydrodynamic interactions. Eur. Phys. J. E. Soft Matter **28**(2), 139–146 (2009)
50. Richard, P., Nicodemi, M., Delannay, R., Ribiere, P., Bideau, D.: Slow relaxation and compaction of granular systems. Nat. Mater. **4**(2), 121 (2005)
51. Risken, H.: Fokker-Planck equation. Springer Berlin Heidelberg, Berlin, Heidelberg (1996)

52. Rosenfeld, Y.: Free-energy model for the inhomogeneous hard-sphere fluid mixture and density-functional theory of freezing. Phys. Rev. Lett. **63**(9), 980 (1989)
53. Roth, R.: Fundamental measure theory for hard-sphere mixtures: a review. J. Phys. Condens. Matter. **22**(6), 063102 (2010)
54. Schneiderbauer, S.: Verification and validation of spatially averaged models for fluidized gas-particle suspensions. Chemical Engineering & Technology **43**(5), 848–858 (2020)
55. Tarazona, P., Cuesta, J.A., Martínez-Ratón, Y.: Density functional theories of hard particle systems. In: Theory and Simulation of Hard-Sphere Fluids and Related Systems, pp. 247–341. Springer (2008)
56. Van Wachem, B.G.M., Almstedt, A.: Methods for multiphase computational fluid dynamics. Chem. Eng. J **96**(1-3), 81–98 (2003)
57. Wilkinson, M.: On global-in-time chaotic weak solutions of the Liouville equation for hard spheres (2018)
58. Wittkowski, R., Löwen, H., Brand, H.R.: Extended dynamical density functional theory for colloidal mixtures with temperature gradients. J. Chem. Phys. **137**(22), 224904 (2012)

A Moments of the collision operator

The moments eqs. (26) and (27) can be constructed analytically by using standard results for moments of Gaussians with mean μ and variance ς:

$$\int_{-\infty}^{\infty} \exp\left(-\frac{(x-\mu)^2}{\varsigma}\right) \mathrm{d}x = \sqrt{\pi}\sqrt{\varsigma}, \quad \int_{-\infty}^{\infty} x \exp\left(-\frac{(x-\mu)^2}{\varsigma}\right) \mathrm{d}x = \sqrt{\pi\varsigma}\mu,$$
$$\int_{-\infty}^{\infty} x^2 \exp\left(-\frac{(x-\mu)^2}{\varsigma}\right) \mathrm{d}x = \frac{\sqrt{\pi\varsigma}}{2}(\varsigma + 2\mu^2),$$

as well as the following identities for integrals of Gaussians over half-infinite domains:

$$\int_{-\infty}^{\infty} \chi_{\pm x>0} \exp\left(-\frac{(x-\mu)^2}{\varsigma}\right) \mathrm{d}x = \frac{\sqrt{\varsigma\pi}}{2}\left(1 \pm \operatorname{erf}\left(\frac{\mu}{\sqrt{\varsigma}}\right)\right),$$
$$\int_{-\infty}^{\infty} \chi_{\pm x>0} x \exp\left(-\frac{(x-\mu)^2}{\varsigma}\right) \mathrm{d}x = \frac{\sqrt{\varsigma\pi}m}{2}\left(1 \pm \operatorname{erf}\left(\frac{\mu}{\sqrt{\varsigma}}\right)\right) \pm \frac{\varsigma}{2}\exp\left(-\frac{\mu^2}{\varsigma}\right),$$
$$\int_{-\infty}^{\infty} \chi_{\pm x>0} x^2 \exp\left(-\frac{(x-\mu)^2}{\varsigma}\right) \mathrm{d}x = \frac{\sqrt{\pi\varsigma}}{2}\left(1 \pm \operatorname{erf}\left(\frac{\mu}{\sqrt{\varsigma}}\right)\right)\left(\frac{\varsigma}{2} + \mu^2\right) \pm \frac{\mu\varsigma}{2}\exp\left(-\frac{\mu^2}{\varsigma}\right),$$
$$\int_{-\infty}^{\infty} \chi_{\pm x>0} x^3 \exp\left(-\frac{(x-\mu)^2}{\varsigma}\right) \mathrm{d}x = \frac{\sqrt{\varsigma\pi}\mu}{2}\left(\frac{3\varsigma}{2} + \mu^2\right)\left(1 \pm \operatorname{erf}\left(\frac{\mu}{\sqrt{\varsigma}}\right)\right)$$
$$\pm\frac{\varsigma}{2}\exp\left(-\frac{\mu^2}{\varsigma}\right)(\mu^2 + \varsigma).$$

The first (un-centred) moment is then zero:

$$\int_{\mathbb{R}} \mathrm{d}p_1 \mathcal{L}_{\mathrm{coll}}\left(f^{(1)}, g^{(2)}, t\right) = 0. \tag{33}$$

We define

$$v^{\pm}_{\mathrm{diff}} = v(r,t) - v(r \pm \sigma, t), \quad v^{\pm}_{\mathrm{sum}} = v(r,t) + v(r \pm \sigma, t), \tag{34}$$
$$E^{\pm}_{\mathrm{diff}} = E(r,t) - E(r \pm \sigma, t), \quad E^{\pm}_{\mathrm{sum}} = E(r,t) + E(r \pm \sigma, t), \tag{35}$$
$$\rho^{\pm} = \rho(r \pm \sigma, t), \quad g_2^{\pm} = g_2(r \pm \sigma, t). \tag{36}$$

The second un-centred moment is then written in terms of error functions:

$$\int_{\mathbb{R}} \mathrm{d}p_1 p_1 \mathcal{L}_{\mathrm{coll}} \left(f^{(1)}, g^{(2)}, t\right) = -\sum_{+,-} \frac{g_2^{\pm}\rho\rho^{\pm}\sqrt{mk_BTE_{\mathrm{sum}}^{\pm}}(1+\alpha)}{2\sqrt{2\pi}} \exp\left(-\frac{m(v_{\mathrm{diff}}^{\pm})^2}{2k_BTE_{\mathrm{sum}}^{\pm}}\right) v_{\mathrm{diff}}^{\pm}$$
$$\pm \frac{g_2^{\pm}\rho\rho^{\pm}(1+\alpha)}{4}\left(1-\mathrm{erf}\left(\frac{\sqrt{m}v_{\mathrm{diff}}^{\pm}}{\sqrt{2k_BTE_{\mathrm{sum}}^{\pm}}}\right)\right)\left(k_BTE_{\mathrm{sum}}^{\pm}+m(v_{\mathrm{diff}}^{\pm})^2\right) \quad (37)$$

And the third un-centred moment is given by

$$\int_{\mathbb{R}} \mathrm{d}p_1 p_1^2 \mathcal{L}_{\mathrm{coll}} \left(f^{(1)}, g^{(2)}, t\right) = -\sum_{+,-} \frac{mg_2^{\pm}\rho\rho^{\pm}\sqrt{mk_BTE_{\mathrm{sum}}^{\pm}}}{2\sqrt{2\pi}} \exp\left(-\frac{(mv_{\mathrm{diff}}^{\pm})^2}{2k_BTE_{\mathrm{sum}}^{\pm}}\right)$$
$$\times\left\{(1+\alpha)\left(2k_BTE_{\mathrm{diff}}^{\pm}+mv_{\mathrm{diff}}^{\pm}v_{\mathrm{sum}}^{\pm}\right)+\frac{1-\alpha^2}{2}\left(2k_BTE_{\mathrm{sum}}^{\pm}+m(v_{\mathrm{diff}}^{\pm})^2\right)\right\}$$
$$\pm\frac{m^2g_2^{\pm}\rho\rho^{\pm}}{4}\left(1-\mathrm{erf}\left(\frac{\sqrt{m}v_{\mathrm{diff}}^{\pm}}{\sqrt{2k_BTE_{\mathrm{sum}}^{\pm}}}\right)\right)$$
$$\times\left\{(1+\alpha)[v_{\mathrm{sum}}^{\pm}(k_BTE_{\mathrm{sum}}^{\pm}+m(v_{\mathrm{diff}}^{\pm})^2)+2k_BTE_{\mathrm{diff}}^{\pm}v_{\mathrm{diff}}^{\pm}]+\frac{1-\alpha^2}{2}v_{\mathrm{diff}}^{\pm}[3k_BTE_{\mathrm{sum}}^{\pm}+m(v_{\mathrm{diff}}^{\pm})^2]\right\} \quad (38)$$

where the sum runs over $+$ and $-$ in place of $\pm$. The centred moments are then constructed as a linear combination of eqs. (33), (37) and (38).

B DDFT using an analytic approximation of g

In [39], an analytic approximation of the radial correlation function is considered, which is independent of α. Although our numeric investigation of the correlation function for different α disagrees with the analytic approximation, for comparison in fig. 10, we provide results using this approximation of g, with the same initial configurations considered in Section 3, in fig. 8. The results show that, under this approximation, the introduction of inelasticity plays a much smaller role in the dynamics. This is in contrast to the large effects seen in the microscopic simulations.

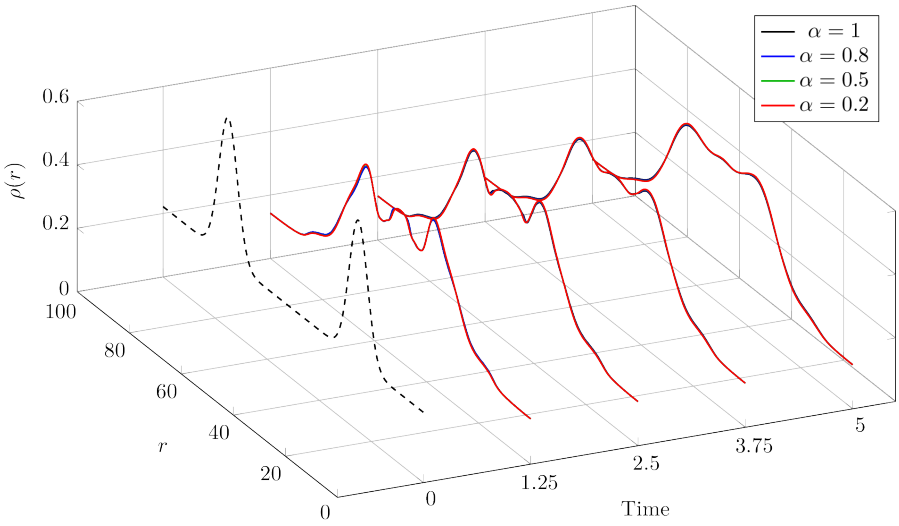

Fig. 10: Results from the DDFT simulation, using $g^{(2)}(\sigma)$ given by eq. (20), using the same initial condition (black, dashed), for different coefficients of restitution α.